Modeling the interaction of DNA with alternating fields

A. E. Bergues-Pupo,[1,2] J. M. Bergues,[3] and F. Falo[2,4]
[1]*Departamento de Física, Universidad de Oriente, 90500 Santiago de Cuba, Cuba*
[2]*Departamento de Física de la Materia Condensada, Universidad de Zaragoza. 50009 Zaragoza, Spain*
[3]*Escuela Politécnica Superior y Facultad de Ciencias de la Salud, Universidad San Jorge, 50830 Villanueva de Gállego, Zaragoza, Spain*
[4]*Instituto de Biocomputación y Física de Sistemas Complejos, Universidad de Zaragoza, 50009 Zaragoza, Spain*
(Received 6 November 2012; published 7 February 2013)

We study the influence of a terahertz field on thermal properties of DNA molecules. A Peyrard-Bishop-Dauxois model with the inclusion of a solvent interaction term is considered. The terahertz field is included as a sinusoidal driven force in the equation of motion. We show how under certain field and system parameters, the melting transition and bubble formation are modified.

DOI: 10.1103/PhysRevE.87.022703 PACS number(s): 87.14.gk, 87.50.U−, 87.16.A−

I. INTRODUCTION

Terahertz (THz) technology and science have spread with evergrowing applications in military and security systems, medicine, biology, and research, e.g., security screening at airports [1,2]; shipment inspection [3]; identification of concealed explosives, drugs, and weapons [2,4,5]; cancer and burn diagnosis [6–11]; and in spectroscopy [6,12,13]. Thus, knowing the effects of THz radiation is critical for different scientific and technological purposes.

Despite the presence of research on the biological effects of THz radiation [14], there are still many controversies. In addition, the emergence of strong sources of THz radiation may contribute to the resolution of controversies over the mechanism of biological organization [15]. The potential of this perspective depends on the development of sophisticated pump-probe and multidimensional experimental techniques and the study of biological systems in the controlled environments necessary for their maintenance and viability [16].

In order to assess the possible genotoxicity of THz radiation with biological materials, in the framework of the THz-BRIDGE project [17], various studies were conducted to investigate the biological response. Recently, a careful analysis of these studies was successfully performed in Ref. [18], in which the authors explored the existence of THz related effects on gene expression that can be unambiguously distinguished from thermal effects. It was suggested that THz radiation may affect gene expression by perturbing the conformational dynamics of double-stranded DNA (dsDNA) [19–21]. These studies were inspired by prior ones [22,23]. As THz photons do not carry enough energy to directly alter chemical reactions, nonlinear resonance effects may cause local changes of breathing dynamics in these systems [24,25].

Motivated by this fact, Alexandrov and co-workers studied the influence of a THz field on the dynamics of a homogeneous poly(A) DNA molecule with 64 base pairs (bps) [19,20]. To model the interactions of dsDNA with the THz field, they made use of the Peyrard-Bishop-Dauxois (PBD) model [26]. They regarded periodic driving and frictional terms in the absence of thermal noise. In that study they found breather modes (localized periodic motions of the double strand) under certain conditions. Hence they concluded that the main effect of THz radiation is to influence resonantly the dynamical stability of the dsDNA. Though Swanson later showed that these breather modes can be eliminated by changing the PBD model parameters or by including thermal noise [27], he agreed that under assumptions concerning drag and drive forcing, breather modes can be generated at certain resonant frequencies.

The PBD model is useful because it allows us to study the equilibrium and dynamic properties of DNA. It has the potential ability to describe the melting transition and denaturation bubbles of the dsDNA such as those that occur during the initial stage of the transcription process. Some specific correlation with transcription initiation sites has been claimed [22,28–31] and debated [32,33].

Tapia-Rojo *et al.* [34] set suitable parameter values for the PBD model and studied the formation and stabilities of bubbles in the system. They used an enhanced model that includes solvent interactions through the addition of a Gaussian barrier to the Morse potential [35]. This barrier modifies the melting transition and the dynamics of the molecule. They also focused on the application of the principal component analysis (PCA) of the trajectories under equilibrium conditions.

Even if both the PBD model and the interaction with an external field taken as Alexandrov and co-workers are quite simple, they could give some insight into the understanding of the interaction of the THz field with the DNA molecule. For this reason our purpose is to study the effect of the THz field on thermal and dynamic properties of DNA: the melting transition and bubble formation at physiological temperatures in the framework of the PBD model. We used a modified version of the model with the inclusion of a solvation barrier and included thermal noise. Both homogeneous and heterogeneous chains are studied in order to deal more closely with reality. The heterogeneous chain is the adeno-associated viral (AAV) P5 promoter (or for simplicity P5 promoter), which has been widely studied [22,29] and plays an important role in the AAV DNA replication [36] and the regulation of the AAV gene expression [37].

This work is divided as follows. In Sec. II we describe the model. In Sec. III the methods are summarized. In Sec. IV an analysis of the response of the system at different frequencies and field amplitudes is made. We show the influence of the THz field, with specific parameters, on the melting transition (Sec. V) and denaturation bubbles (Sec. VI). A summary is provided in Sec. VII.

II. MODEL

The PBD model is a mesoscopic dynamical model of the DNA molecule. It describes the stretching of the bonds between the bps through a single variable, which condenses all the atomic coordinates of a bp. This model ignores the helicoidal structure and uses the Morse potential to model hydrogen bonding between bps. A nonlinear interpair stacking potential is also considered. We use a modification of the PBD model including a solvation barrier inside the Morse potential. This barrier prevents the closing of the base once it is opened. The total energy of the system is then approached by

$$H = \sum_n \left[\frac{p_n^2}{2m} + V(y_n) + W(y_n, y_{n-1}) \right]. \quad (1)$$

In this equation $V(y_n)$ is an on-site potential that describes the interaction between the two bases of a pair. It is represented by the Morse potential and a Gaussian barrier is added:

$$V(y) = D(e^{-\alpha y} - 1)^2 + Ge^{-(y-y_0)^2/b}. \quad (2)$$

The parameters D, α, G, y_0, and b are sequence dependent. Following Ref. [38], in our simulations we use $D_{CG} = 1.5D_{AT}$ and $\alpha_{CG} = 1.5\alpha_{AT}$. Here D is the bp dissociation energy and α sets the amplitude of the potential well. The barrier height is controlled by G and its position and its width are given by y_0 and b, respectively. A reasonable selection for such parameters is $G = 3D$, $y_0 = 2/\alpha$, and $b = 1/2\alpha^2$ [34]. The term $W(y_n, y_{n-1})$ accounts for the stacking interactions and is given by

$$W(y_n, y_{n-1}) = \tfrac{1}{2}K(1 + \rho e^{-\delta(y_n + y_{n-1})})(y_n - y_{n-1})^2. \quad (3)$$

The effect of this term, whose intensity is governed by ρ, is to change the effective coupling constant from $K(1+\rho)$ to K when one of the bps is displaced far from its equilibrium position. The parameter δ sets the scale length for this behavior. Alternatively, the inhomogeneous stacking energy can be also considered [39].

We use the same value parameters of the PBD model with the solvation barrier that appear in Ref. [34]: $D_{AT} = 0.051\,85$ eV, $G_{AT} = 0.1556$ eV, $y_{0AT} = 0.5$ Å, $b_{AT} = 0.031\,25$ Å^2, $K = 0.03$ eV Å^2, $\rho = 3$, and $\delta = 0.8$ Å^{-1}.

III. METHODS

In order to study the behavior of the system we have performed molecular-dynamics numerical simulations of the Langevin equation

$$m\frac{\partial^2 y_n}{\partial t^2} + m\gamma\frac{\partial y_n}{\partial t} = -\frac{\partial[W(y_n, y_{n+1} + W(y_{n-1}, y_n)]}{\partial y_n} - \frac{\partial V}{\partial y_n} + \xi_n(t) + A\cos(\omega t), \quad (4)$$

where m is the mass of the bp, γ is the effective damping of the system, $\xi(t)$ accounts for thermal noise, $\langle \xi_n(t) \rangle = 0$, $\langle \xi_n(t)\xi_k(t') \rangle = 2m\gamma k_B T \delta_{nk}\delta(t - t')$, T is the bath temperature, and A and ω are the field amplitude and frequency, respectively. The equations are numerically integrated using a stochastic Runge-Kutta algorithm [40,41]. We thermalize for 200 ps without field and 200 ps with field before any record is made. Simulations of the melting transition are performed using periodic boundary conditions, while those of thermal bubbles with fixed boundary conditions are as in Ref. [34]. The P5 promoter is given by the 69 bps: 5′-GTGCCCATTTAGGGTATATATGGCCGAGTGAGCGAG CAGGATCTCCATTTTGACCGCAAATTTGAACG-3′. For methodological issues we analyze homogeneous chains as well. In these cases the chains have the same number of bps as the P5 chain.

To show the influence of field parameters in the system response we use the mean displacement $\langle y \rangle$ defined as

$$\langle y \rangle = \frac{1}{Nt_s}\sum_{n,t}^{N,t_s} y_n(t), \quad (5)$$

where N is the number of bps and t_s is the simulation time. For the melting transition we also measure the mean energy $\langle u \rangle$ as a function of the temperature

$$\langle u \rangle = \frac{1}{Nt_s}\sum_{n,t}^{N,t_s}[W(y_n - y_{n-1}) + V(y_n)]. \quad (6)$$

In order to calculate the opening probability and lifetime of a bubble we follow Ref. [22]. The probability $P_n(l, \mathcal{V}_{\rm tr})$ for the existence of a bubble of certain length l of bps, threshold $\mathcal{V}_{\rm tr}$, and beginning at the nth bp is calculated as

$$P_n(l, \mathcal{V}_{\rm tr}) = \frac{1}{t_s}\sum_{a=1}^{q_n^{\max}(l,\mathcal{V}_{\rm tr})} \Delta t[q_n(l, \mathcal{V}_{\rm tr})], \quad (7)$$

where $q_n(l, \mathcal{V}_{\rm tr})$ counts for the bubbles of duration $\Delta t[q_n(l, \mathcal{V}_{\rm tr})]$. The average bubble duration τ is calculated as the average time of a bubble of a given shape over all occurrences of that bubble,

$$\tau_n = \frac{\sum_{a=1}^{q_n^{\max}(l,\mathcal{V}_{\rm tr})} \Delta t[q_n(l, \mathcal{V}_{\rm tr})]}{\sum_{a=1}^{q_n^{\max}(l,\mathcal{V}_{\rm tr})}[q_n(l, \mathcal{V}_{\rm tr})]}. \quad (8)$$

We can extract information from a large set of data in a multidimensional phase space through the PCA. It allows us to reduce the dimensionality of the variable to those that include most of the fluctuations of the original system [42]. From an operational point of view, we have to build the $N \times N$ correlation matrix. Thus

$$C(i, j) = \langle y_i y_j \rangle - \langle y_i \rangle \langle y_j \rangle. \quad (9)$$

The diagonalization of this matrix allows us to obtain an ordered set of eigenvalues $(\lambda_1 > \lambda_2 > \lambda_3 > \cdots)$ with their corresponding eigenvectors $(v_1, v_2, v_3, \ldots)$. The number of fluctuations is given by the eigenvalues. The new coordinates are ordered in such a way that most of the system fluctuations are retained by the first few.

IV. SYSTEM RESPONSE FOR DIFFERENT FREQUENCIES AND FIELD AMPLITUDES

Before performing the simulations for the melting transition and bubble formation, some preliminary steps should be done. First, we look for the frequency values at which maximum responses are obtained for each sequence. These values depend on temperature. At low temperatures they should be on

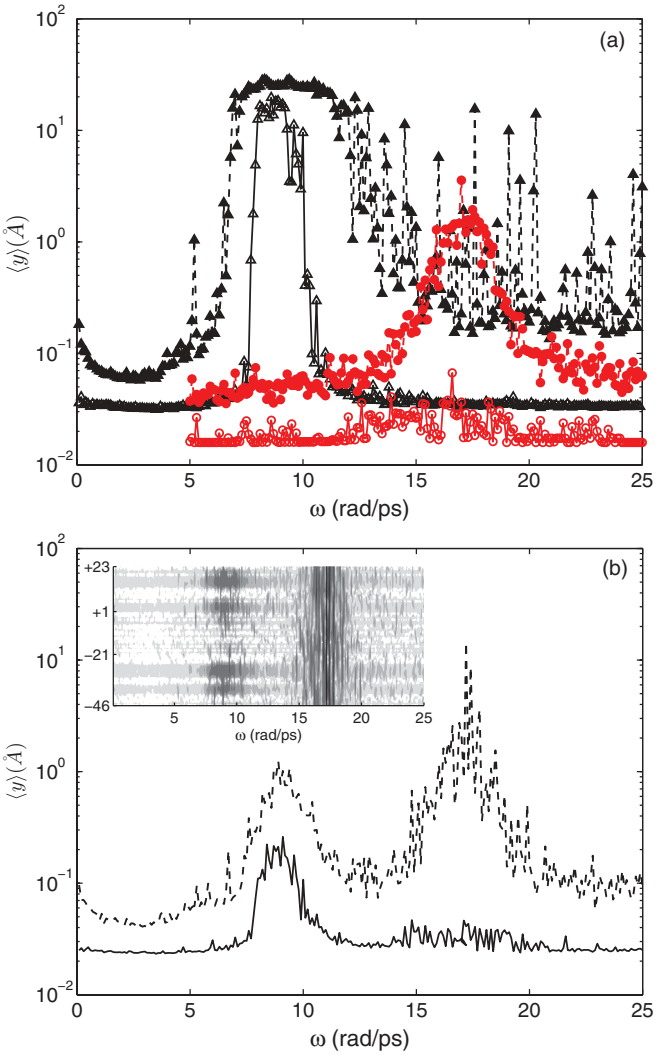

FIG. 1. (Color online) Frequency dependence of $\langle y \rangle$ with $A = 50$ pN and $\gamma = 1$ ps^{-1}. (a) The AT chain is represented by lines with triangles and the CG one by circles. Solid markers are for $T = 290$ K and open are for $T = 210$ K. (b) The P5 promoter. The solid line is for $T = 210$ K and the dashed line for $T = 290$ K. The inset shows the frequency dependence of $\langle y \rangle$ for each base at $T = 290$ K.

the order of the linear resonances of the system. Nonlinear oscillations become important at intermediate temperatures, while above the melting temperature, frequency values belong to those of a Gaussian chain.

The system dynamics depends on damping values as well. Thus we consider two values for the damping coefficient $\gamma = 1$ and 9.8 ps^{-1}. Figure 1 shows the behavior of three sequences with 69 bps. The calculation is performed with a field amplitude $A = 50$ pN, damping factor $\gamma = 1$ ps^{-1}, and two temperature values $T = 210$ and 290 K.

Maximum responses occur at certain frequency values, even for large field amplitudes (not shown). Some modes are activated when the temperature increases (see Fig. 1). The frequency bandwidth slightly increases when temperature rises. These bands are around $\omega = 9$ and 17 rad/ps for AT and CG chains, respectively. The increased of $\langle y \rangle$ for certain frequency values could lead to bubble formation or the full

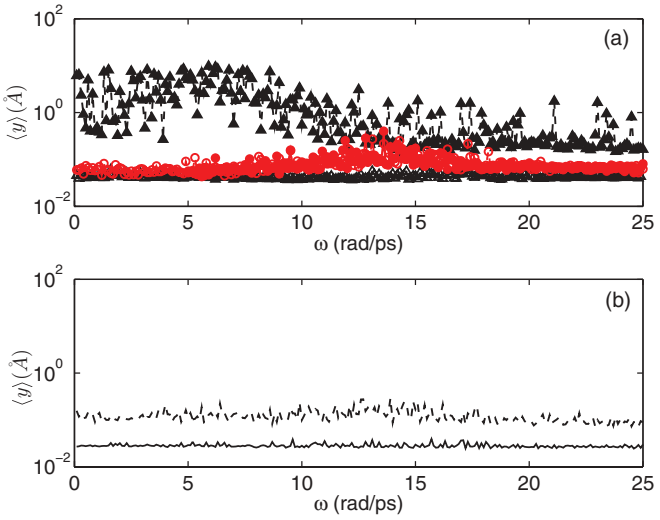

FIG. 2. (Color online) Frequency dependence of $\langle y \rangle$ with $A = 144$ pN and $\gamma = 9.8$ ps^{-1}. (a) The AT chain is represented by lines with triangles and the CG one by circles. Solid markers are for $T = 290$ K and open are for $T = 210$ K. (b) The P5 promoter. The solid line is for $T = 210$ K and the dashed line for $T = 290$ K.

melting. The resonant frequencies of the P5 promoter are the same as those for the AT and CG chains. In other words, the P5 promoter behaves as if it would be composed of two homogeneous chains on the frequency space. This behavior may be understood because the numbers of AT and CG bps on the chain are approximately equal. However, the $\langle y \rangle$ values are less than those corresponding to the homogenous sequences. At $T = 210$ K the maximum response for the P5 promoter occurs around $\omega = 9$ rad/ps. Only the AT bases are stimulated and for this reason localized openings are observed around the AT richer regions [see the inset of Fig. 1(b)]. At $T = 290$ K the maximum response occurs at both $\omega = 9$ and 17 rad/ps. The CG bases are also stimulated. In this case, there is enough energy to open AT bases as well due to stacking interactions and the whole chain opens. Figure 2 illustrates the frequency dependence of $\langle y \rangle$ with $\gamma = 9.8$ ps^{-1}. With a larger damping, it is no longer possible to obtain resonant frequencies because the stochastic term becomes dominant.

We also calculate the amplitude dependence of $\langle y \rangle$ to determine A values for the following simulations. The frequency values of the maximum responses are used: $\omega = 9$ rad/ps for the AT and P5 chains and $\omega = 17$ rad/ps for the CG chain. Results for $\omega = 17$ rad/ps for the P5 chain are similar to those of $\omega = 9$ rad/ps. Figures 3 and 4 show the results for $\gamma = 1$ and 9.8 ps^{-1}, respectively.

According to Fig. 3 for $\gamma = 1$ ps^{-1}, we can use $A = 10$, 25, and 50 pN for the three chains. In the case of $\gamma = 9.8$ ps^{-1} the values are $A = 50$, 144, and 200 pN.

V. MELTING TRANSITION

This section focuses on the study of the melting transition of the homogeneous chains and P5 promoter. Our goal is to analyze how a THz field modifies the melting temperature T_m and the transition width ΔT. These parameters were determined in Ref. [34] for the uniform chain of AT bps

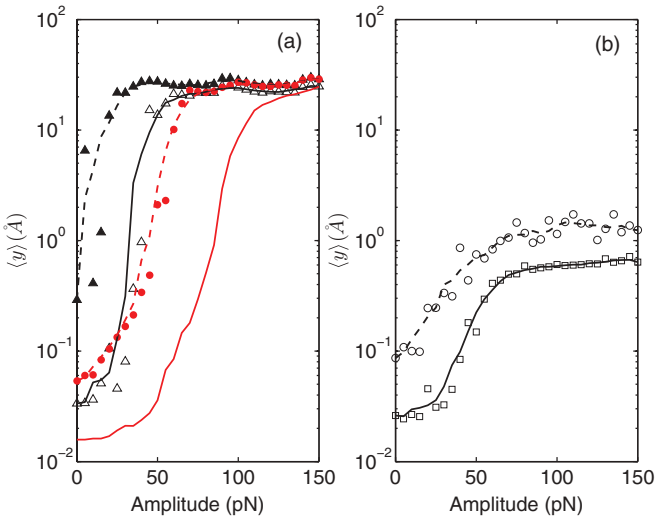

FIG. 3. (Color online) Amplitude dependence of $\langle y \rangle$ with $\gamma = 1$ ps^{-1}. (a) The AT chain is represented by triangles and the CG one by circles. Solid markers are for $T = 290$ K and open are for $T = 210$ K. (b) The P5 promoter. Squares are for $T = 210$ K and circles for $T = 290$ K. Lines are a guide for the eye.

without external field. Following the same criteria, we can determine them when the external field is applied. We calculate the mean potential energy and mean displacement as a function of the temperature. We determine the two temperatures as follows. The temperature T_1 estimates the beginning of the transition where $\langle y(T) \rangle$ crosses 0.5 Å. The larger one T_2 provides the onset of the linear behavior in $\langle y(T) \rangle$. Both quantities are defined in the forms $T_m = (T_1 + T_2)/2$ and $\Delta T = (T_2 - T_1)/2$. Figure 5 displays melting transition curves for the AT chain and P5 promoter. Melting transition curves for the CG and P5 chains at $\omega = 17$ rad/ps have similar behaviors (not shown).

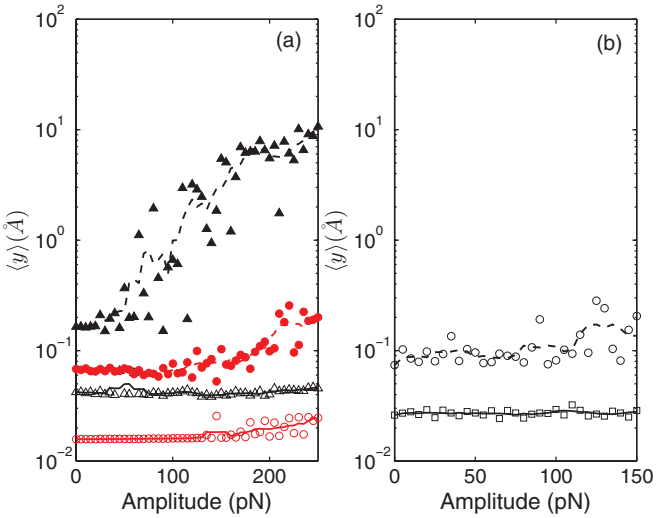

FIG. 4. (Color online) Amplitude dependence of $\langle y \rangle$ with $\gamma = 9.8$ ps^{-1}. (a) The AT chain is represented by triangles and the CG one by circles. Solid markers are for $T = 290$ K and open are for $T = 210$ K. (b) The P5 promoter. Squares are for $T = 210$ K and circles for $T = 290$ K. Lines are a guide for the eye.

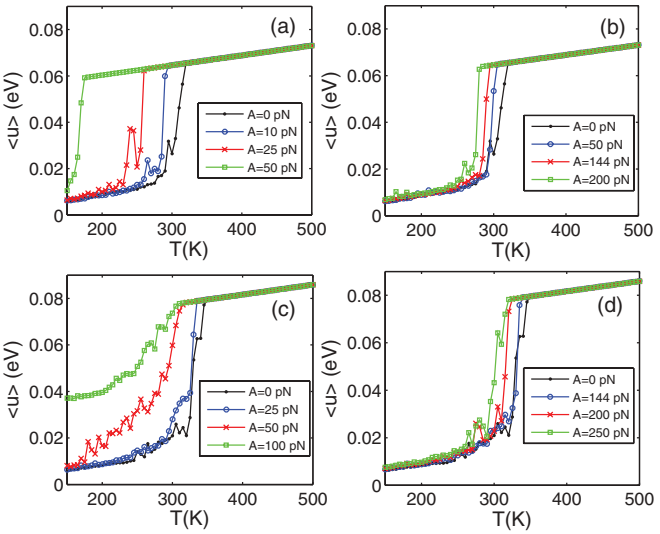

FIG. 5. (Color online) Melting transition at the frequency $\omega = 9$ rad/ps. (a) The AT chain with damping factor $\gamma = 1$ ps^{-1}, (b) the AT chain with damping factor $\gamma = 9.8$ ps^{-1}, (c) the P5 chain with damping factor $\gamma = 1$ ps^{-1}, and (d) the P5 chain with damping factor $\gamma = 9.8$ ps^{-1}.

While the mean potential energy curves coincide above T_2 for different field amplitude and damping values, the mean displacement curves differ. This can be explained because the action of the field is such that the difference $y_n - y_{n-1}$ between two successive bps at each time step remains constant. In this region the potential energy depends only on the difference $y_n - y_{n-1}$. Figure 6 shows the behavior of the melting transition temperature versus field amplitude for the three chains.

The differences between the melting transition with and without an applied field are remarkable (see Figs. 5 and 6). Due to the applied external field, the chains melt at lower temperatures. This fact has been already noted by Swanson

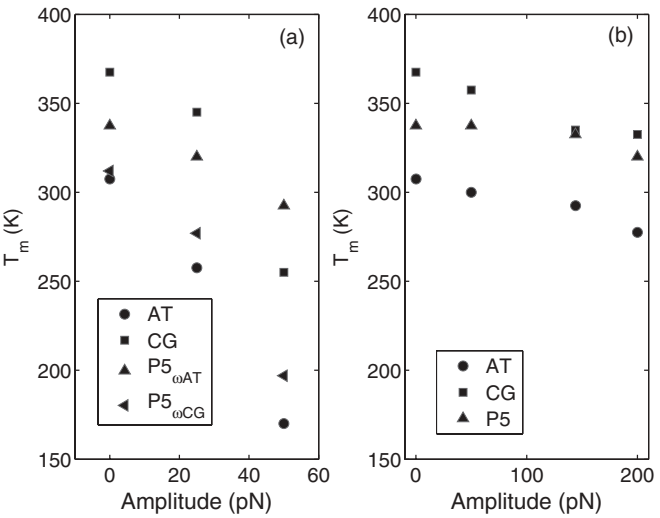

FIG. 6. (Color online) Melting transition temperature. (a) Damping factor $\gamma = 1$ ps^{-1} and frequency $\omega = 9$ rad/ps for the AT and P5 chains (P5$_{\omega AT}$) and $\omega = 17$ rad/ps for the CG and P5 chains (P5$_{\omega CG}$). (b) Damping factor $\gamma = 9.8$ ps^{-1} and frequency $\omega = 9$ rad/ps for the AT and P5 chains and $\omega = 17$ rad/ps for the CG chain.

[27] for a homogeneous chain. In contrast to that work, the values of T_m we obtain here are larger than the one reported therein. The behavior of the transition width is more complex because it depends on the number of bps that have been opened at a certain temperature. The field allows both opening and closing of bps. For $\gamma = 9.8$ ps^{-1} the effect of the field decreases and larger values of field amplitude are needed to lower the transition temperature.

VI. BUBBLE FORMATION

We now study the THz field influence on the bubble formation at $T = 290$ K with the parameters chosen as in the preceding section. This temperature belongs to the premelting range, in which it has been shown that the highest opening probability coincides with important biological sites such as the start transition site (TSS) and the TATA box [28–30]. In order to avoid unphysical denaturation process due to finite-size effects, we add a sequence of 10 CG bps to the ends of the P5 promoter to create hard boundaries. The extremes are set to zero, avoiding the complete opening of the chain [34]. Figures 7 and 8 show the bubble size and

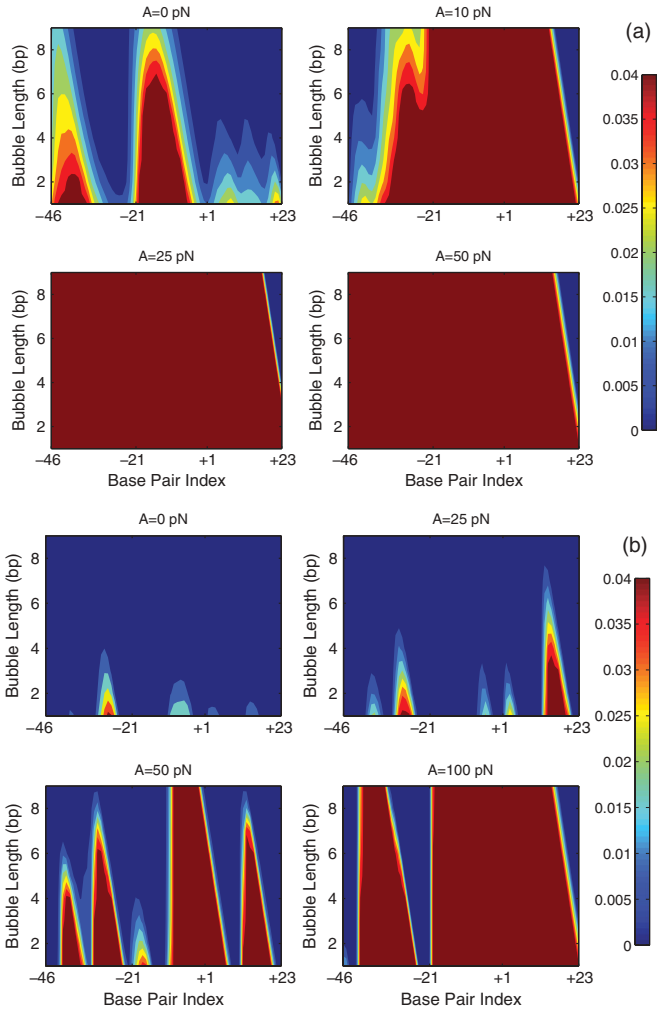

FIG. 7. (Color online) Probability opening distribution P_n with frequency $\omega = 9$ rad/ps, damping factor $\gamma = 1$ ps^{-1}, and $T = 290$ K for the (a) AT chain and (b) P5 promoter.

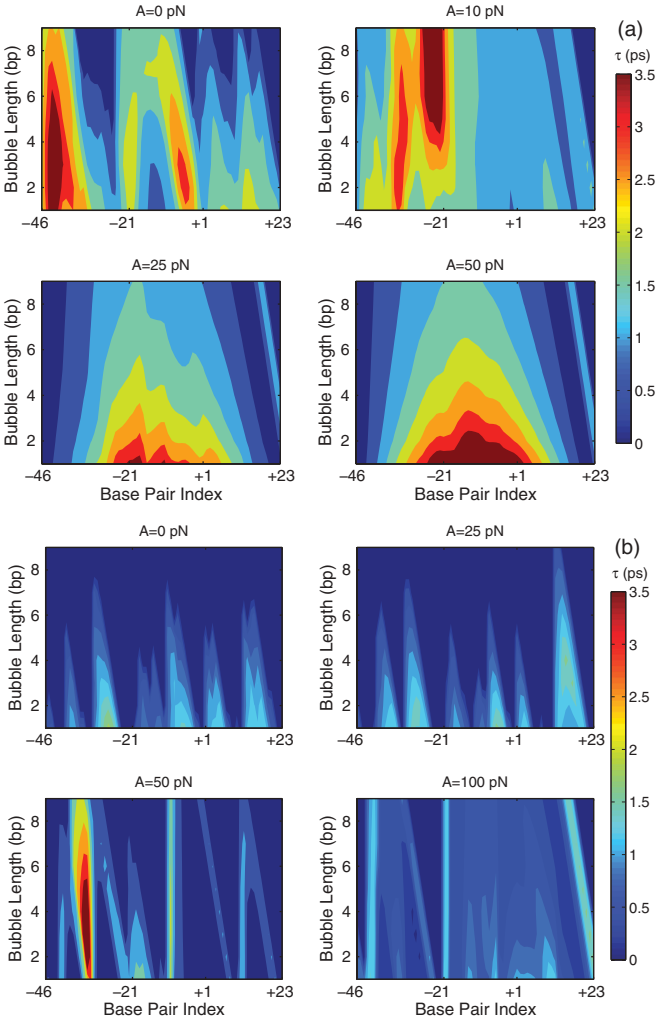

FIG. 8. (Color online) Average lifetime distribution τ_n with frequency $\omega = 9$ rad/ps, damping factor $\gamma = 1$ ps^{-1}, and $T = 290$ K for the (a) AT chain and (b) P5 promoter.

lifetime distribution, respectively, for the AT chain and P5 promoter with $\omega = 9$ rad/ps and $\gamma = 1$ ps^{-1}. Here P_n and τ_n, given by Eqs. (7) and (8), are defined with a threshold value of $\mathcal{V}_{\rm tr} = 1.5$ Å. These magnitudes are represented as a function of the bubble length and index site. The opening probability and bubble lifetime are given in color scale. In these figures the 10 bps at the beginning and the end of the sequence are not included. The +1 in the base pair index refers to the TSS position in the P5 promoter. In the homogeneous chain there is no TSS, but we keep the same notation for convenience.

Figure 7 shows how the external field enhances the opening probability at the frequency value $\omega = 9$ rad/ps. Results agree with those of the melting transition. Without a field, the larger probabilities in the P5 promoter occur in two sites of biological interest, as previously reported: the TSS (represented by +1) and the TATA box (between −30 and −40). Increasing the field amplitude leads to the increase of opening probability at these sites and helps the opening of others. Without the THz field, the opening probability of the P5 promoter at the TATA box is higher than at the TSS [31,43]. The most persistent bubbles are found at the sites that have been pointed out before (see Fig. 8).

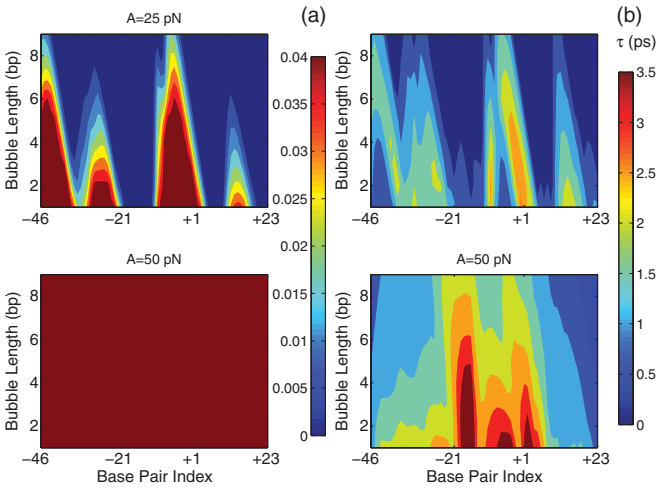

FIG. 9. (Color online) Probability opening distribution P_n and average lifetime distribution τ_n for the P5 promoter with frequency $\omega = 17$ rad/ps, damping factor $\gamma = 1$ ps^{-1}, and $T = 290$ K for $A = 25$ pN (top) and $A = 50$ pN (bottom).

In our simulations, the lifetime values depend on the selection of the parameters of the modified PBD model. Thus the results in some cases can be different with respect to those reported in the literature when the THz field is not applied. For the AT chain, the field makes bubbles more stable, but for the P5 promoter it does not. In this case, the heterogeneity of the chain plays a crucial role because we use $\omega = 9$ rad/ps. The decrease of bubble lifetime may be explained because the energy of the field favors both opening and closing events of the bps. The opening and closing kinetics is governed by the solvation barrier and the applied field. With a barrier and without an applied field, the kinetics is controlled by the presence of two equilibrium states separated by the solvation barrier. Closing events are more difficult and bubbles exist longer than those in which the barrier is not considered [34]. In contrast, at this frequency the CG bps are not stimulated. If we use $\omega = 17$ rad/ps, the CG bps are stimulated and the whole chain opens, as explained previously (Fig. 9). The same calculations are performed with $\gamma = 9.8$ ps^{-1} (not shown). As in previous results, the damping factor modifies the chain dynamics and high field amplitude values are needed to open the chain.

Finally, we compare the results obtained from the PCA with the average displacement values of each base (see Fig. 10). The 10 CG bps at the ends of the sequence are included in the figures. We show the results for only the P5 promoter with a field amplitude of $A = 50$ pN.

A good correlation between the top and bottom figures is verified. Localized eigenvectors span over regions of nine bps, which corresponds fairly to the width of the bubbles, as in Ref. [34]. For other field amplitudes and the homogeneous chains there is a good correlation too.

Our results suggest that the THz field influence can be viewed in two main directions. First, the applied field tends to facilitate melting and bubble formation, which could in principle affect processes such as transcription or replication. The driving forces needed to observe such effects are large compared with those found in physically reliable conditions for *in vivo* exposure [27]. We do not disagree with this conclusion.

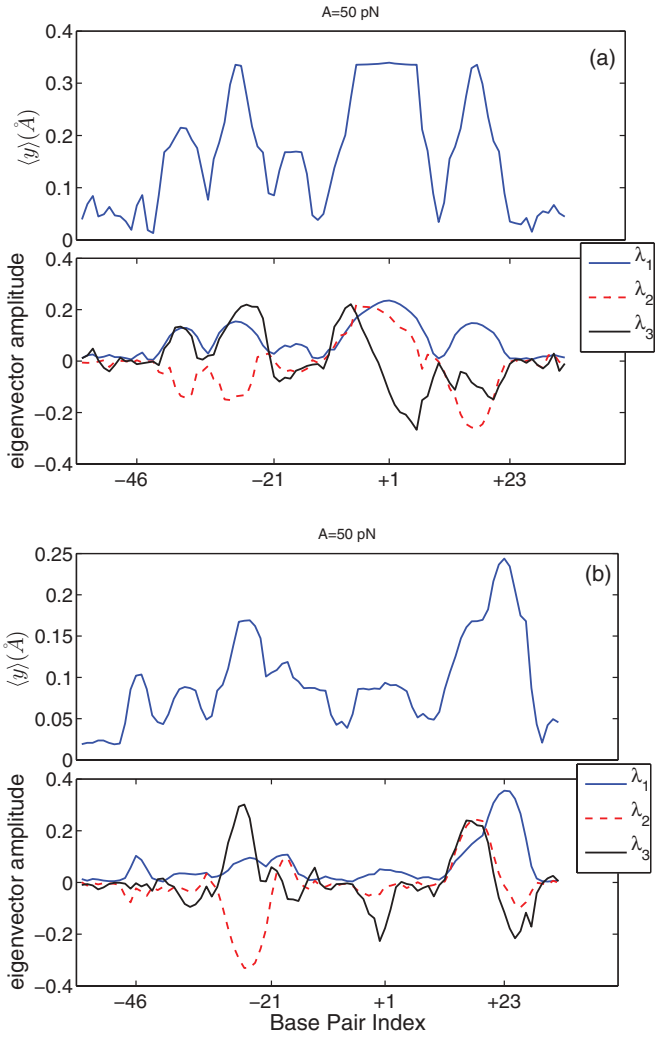

FIG. 10. (Color online) Probability of opening for the P5 promoter (top) and the first three PC eigenvectors corresponding to eigenvalues λ_1, λ_2, and λ_3 at $T = 290$ K for (a) $\gamma = 1$ ps^{-1} and (b) $\gamma = 9.8$ ps^{-1}.

We have just used a simple model for such a description and the magnitude values may not match the real ones. Second, the external field could be used to detect biologically significant sites by increasing the opening probability at these sites without the melting of the chain. In this scenario the effective drive could be larger.

VII. CONCLUSION

We have studied in the framework of the PBD model the influence of the THz field on homogeneous chains and the heterogeneous P5 promoter. Thermal properties of these sequences have been studied by including thermal noise and a solvation barrier in the model. The influence of the THz field depends strongly on field parameters (frequency and field amplitude) and system parameters (potential parameters and damping). In spite of previous results, we do not obtain breather modes (oscillatory solutions), but rather we find that ac fields favor the formation of bubbles.

We have also identified the frequency resonant bands that mostly increase the opening of the chain. The positions of the bands are sequence dependent and distinguish the AT-rich regions from CG-rich regions. This could increase the experimental resolution in order to detect sites such as the TSS if small field amplitudes are used. Further study in this direction needs to be done, for instance, considering more complex interaction between bases and the external field. Finally, we have numerically obtained that the PCA can also be used to get information for out-of-equilibrium systems.

ACKNOWLEDGMENTS

We thank R. Tapia-Rojo for assistance with model parameters and a critical reading of the manuscript. The work was supported by the Spanish Project No. FIS2011-25167 cofinanced by Fondo Europeo de Desarrollo Regional funds.

[1] R. Appleby and H. B. Wallace, IEEE Trans. Antennas Propag. **55**, 2944 (2007).
[2] J. F. Federici, B. Schulkin, F. Huang, D. Gary, R. Barat, F. Oliveira, and D. Zimdars, Semicond. Sci. Technol. **20**, 266 (2005).
[3] D. Zimdars and J. S. White, in *Terahertz for Military and Security Applications II*, Proceedings of the SPIE Vol. 5411, Orlando, 2004, edited by R. J. Hwu and D. L. Woolard (SPIE, Bellingham, WA, 2004), p. 78.
[4] R. Bogue, Sensor Rev. **29**, 6 (2009).
[5] A. Dobroiu, C. Otani, and K. Kawase, Meas. Sci. Technol. **17**, 161 (2006).
[6] P. C. Ashworth, E. Pickwell-MacPherson, E. Provenzano, S. E. Pinder, A. D. Purushotham, M. Pepper, and V. P. Wallace, Opt. Express **17**, 12444 (2009).
[7] M. A. Brun, F. Formanek, A. Yasuda, M. Sekine, N. Ando, and Y. Eishii, Phys. Med. Biol. **55**, 4615 (2010).
[8] S. J. Oh, J. Kang, I. Maeng, J. S. Suh, Y. M. Huh, S. Haam, and J. H. Son, Opt. Express **17**, 3469 (2009).
[9] V. P. Wallace, P. F. Taday, A. J. Fitzgerald, R. M. Woodward, J. Cluff, R. J. Pye, and D. D. Arnone, Faraday Discuss. **126**, 255 (2004).
[10] Z. D. Taylor, R. S. Singh, M. O. Culjat, J. Y. Suen, W. S. Grundfest, H. Lee, and E. R. Brown, Opt. Lett. **33**, 1258 (2008).
[11] R. M. Woodward, B. E. Cole, V. P. Wallace, R. J. Pye, D. D. Arnone, E. H. Linfield, and M. Pepper, Phys. Med. Biol. **47**, 3853 (2002).
[12] P. U. Jepsen, U. Moller, and H. Merbold, Opt. Express **15**, 14717 (2007).
[13] L. Thrane, R. H. Jacobsen, P. U. Jepsen, and S. R. Keiding, Chem. Phys. Lett. **240**, 330 (1995).
[14] G. J. Wilmink and J. E. Grundt, J. Infrared Milli. Terahz. Waves **32**, 1074 (2011).
[15] P. Weightman, *Proceedings of the Joint 32nd International Conference on Infrared and Millimeter Waves and the 15th International Conference on Terahertz Electronics, Cardiff, 2007*, IEEE No. 07EX1863C (IEEE, Piscataway, NJ, 2007), pp. 1–3.
[16] P. Weightman, Phys. Biol. **9**, 053001 (2012).
[17] THz-BRIDGE Project (2004), http://www.frascati.enea.it/THz-BRIDGE/.
[18] B. S. Alexandrov, K. O. Rasmussen, A. R. Bishop, A. Usheva, L. B. Alexandrov, S. Chong, Y. Dagon, L. G. Booshehri, Ch. H. Mielke, M. L. Phipps, J. S. Martinez, H. T. Chen, and G. Rodriguez, Biomed. Opt. Express **9**, 2679 (2011).
[19] B. S. Alexandrov, V. Gelev, A. R. Bishop, A. Usheva, and K. O. Rasmussen, Phys. Lett. A **374**, 1214 (2010).
[20] P. Maniadis, B. S. Alexandrov, A. R. Bishop, and K. O. Rasmussen, Phys. Rev. E **83**, 011904 (2011).
[21] J. Bock, Y. Fukuyo, S. Kang, M. L. Phipps, L. B. Alexandrov, K. O. Rasmussen, A. R. Bishop, E. D. Rosen, J. S. Martinez, H. T. Chen, G. Rodriguez, B. S. Alexandrov, and A. Usheva, PLoS ONE **5**, 15806 (2010).
[22] B. S. Alexandrov, V. Gelev, S. W. Yoo, A. R. Bishop, K. O. Rasmussen, and A. Usheva, PLoS Comput. Biol. **5**, 1000313 (2009).
[23] B. S. Alexandrov, V. Gelev, S. W. Yoo, L. B. Alexandrov, Y. Fukuyo, A. R. Bishop, K. O. Rasmussen, and A. Usheva, Nucleic Acids Res. **38**, 1790 (2010).
[24] M. Blank and R. Goodman, Bioelectromagnetics **18**, 111 (1997).
[25] B. M. Fischer, M. Walther, and P. Uhd Jepsen, Phys. Med. Biol. **47**, 3807 (2002).
[26] T. Dauxois, M. Peyrard, and A. R. Bishop, Phys. Rev. E **47**, 684 (1993).
[27] E. S. Swanson, Phys. Rev. E **83**, 040901 (2011).
[28] C. H. Choi, G. Kalosakas, K. O. Rasmussen, M. Hiromura, A. R. Bishop, and A. Usheva, Nucleic Acids Res. **32**, 1584 (2004).
[29] G. Kalosakas, K. O. Rasmussen, A. R. Bishop, C. H. Choi, and A. Usheva, Europhys. Lett. **68**, 127 (2004)
[30] C. H. Choi, Z. Rapti, V. Gelev, M. R. Hacker, B. S. Alexandrov, E. J. Park, J. S. Park, N. Horikoshi, A. Smerzi, K. O. Rasmussen, A. R. Bishop, and A. Usheva, Biophys J. **95**, 597 (2008).
[31] B. S. Alexandrov, L. T. Wille, K. O. Rasmussen, A. R. Bishop, and K. B. Blagoev, Phys. Rev. E **74**, 050901 (2006).
[32] C. H. Choi, A. Usheva, G. Kalosakas, K. O. Rasmussen, and A. R. Bishop, Phys. Rev. Lett. **96**, 239801 (2006); T. S. van Erp, S. Cuesta-Lopez, J.-G. Hagmann, and M. Peyrard, *ibid.* **96**, 239802 (2006).
[33] T. S. van Erp, S. Cuesta-Lopez, and M. Peyrard, Eur. Phys. J. E **20**, 421 (2006).
[34] R. Tapia-Rojo, J. J. Mazo, and F. Falo, Phys. Rev. E **82**, 031916 (2010).
[35] G. Weber, Phys. Europhys. Lett. **73**, 806 (2006).
[36] J. D. Tratschin, I. L. Miller, and B. J. Carter, J. Virol. **51**, 611 (1984).
[37] M. A. Labow, P. L. Hermonat, and K. I. Berns, J. Virol. **60**, 251 (1984).
[38] A. Campa and A. Giansanti, Phys. Rev. E **58**, 3585 (1998).
[39] G. Weber, J. W. Essex, and C. Neylon, Nat. Phys. **5**, 769 (2009).
[40] H. S. Greenside and E. Helfand, Bell Syst. Tech. J. **60**, 1927 (1981).
[41] E. Helfand, Bell Syst. Tech. J. **58**, 2289 (1979).
[42] I. T. Jolliffe, *Principal Components Analysis*, 2nd ed. (Springer, New York, 2002).
[43] T. S. van Erp, S. Cuesta-Lopez, J.-G. Hagmann, and M. Peyrard, Phys. Rev. Lett. **95**, 218104 (2005).